Insights into the Catalytic Mechanism of Chlorothalonil Hydrolytic Dehalogenase

Xinhang Yang, ¹ Brian Bennett, ² and Richard C. Holz. ^{1,3*}

¹Department of Chemistry, Marquette University, PO Box 1881, Milwaukee, Wisconsin 53201-1881, ²Department of Physics, Marquette University, 1420 W. Clybourn St., Milwaukee, Wisconsin 53233 and the ³Department of Chemistry, Colorado School of Mines, Golden, Colorado 80401

Running Title: Hydrolytic Dehalogenase

To whom correspondence should be addressed: Richard C. Holz, Department of Chemistry, Colorado School of Mines, Golden, Colorado 80401, Phone: 303-273-3003, E-mail: rholz@mines.edu

Keyword: Chd, Enzyme Kinetics, Zinc, Stopped-Flow

ABSTRACT

A direct spectrophotometric assay for the Zn(II)dependent chlorothalonil hydrolytic dehalogenase from Pseudomonas sp. CTN-3 (Chd) was developed, which allowed the metal binding properties, the pH dependence of the kinetic parameters k_{cat} , K_{m} , and k_{cat} / $K_{\rm m}$, and the solvent isotope effect to be determined. A single Zn(II) ion was found to bind per Chd monomer with a K_d of 0.17 μ M, consistent with ICP-MS data for the as-isolated Chd dimer. Maximum activity toward chlorothalonil was observed in the pH range 7.0 to 9.0 and fits of these data provided a p $K_{\rm ES1}$ value of 5.4 ± 0.2 , a p K_{ES2} value of 9.9 ± 0.1 ($k'_{cat} = 24$ \pm 2 s⁻¹), a p K_{E1} value of 5.4 \pm 0.3, and a p K_{E2} value of $9.5 \pm 0.1 (k'_{cat}/K'_{m} = 220 \pm 10 \text{ s}^{-1}\text{mM}^{-1})$. Proton inventory studies indicated that one proton is transferred in the rate-limiting step of the reaction at pD 7.0. Fits of UV-Vis stopped-flow data suggest a three-step mechanism. The apparent rate constants for intermediate formation, $k_2 = 35.2 \pm 0.1 \text{ s}^{-1}$ and product release $k_3^{'}$ = 1.1 ± 0.2 s⁻¹ were determined indicating that product release is the slow-step in catalysis. The combination of these data, along with those previously reported, allowed a catalytic mechanism for Chd to be proposed for the first time.

Chlorothalonil (TPN; 2,4,5,6-tetrachloroisophtalonitrile) is one of the most commonly used fungicides in the US with more than five million kilograms sprayed on crops and fruits each year (1-4). TPN has low solubility in water (100 mg L⁻¹) but it is strongly absorbed in soil, particularly soil with high organic matter such as those found in aquatic environments. It is stable to hydrolysis between pH 5 to 7, with a half-life of 30 to 60 days, and it can remain in soil for over a year (5). It is highly toxic to fish and aquatic species as well as birds and invertebrates and is emerging as a major environmental issue (6,7). TPN is also a human skin and eye irritant that can cause severe gastrointestinal issues. Animal studies involving mice have shown that TPN can cause kidney cancer, so it has been classified by the U.S. Environmental Protection Agency (EPA) as a probable human carcinogen (3). Given the widespread use of TPN and its toxicity, its biodegradation and environmental clean-up has become a topic of significant importance (8).

Characterized pathways for biological dehalogenation of organics include oxidative, reductive, and thiolytic mechanisms (9-15). However, selective partial dehalogenation of TPN can

also be catalyzed by a hydrolytic process that converts TPN to 4-hydroxytrichloroisophthalo-nitrile (4-OH-TPN) and chloride (Scheme 1)

Scheme 1. The hydrolysis of TPN to 4-OH-TPN and chloride by Chd.

$$\begin{array}{c|c} & & & \\ &$$

(7,16,17). Several bacterial strains harbor a gene that has been shown to be responsible for TPN dehalogenation (18-20). Each of these gene products exhibit remarkable (>95%) identity and require Zn(II) as a cofactor for catalysis (Figure 1).

The best characterized enzyme within this group is the chlorothalonil (TPN) dehalogenase from pseudomonas sp. CTN-3 (Chd, EC:3.8.1.2) (7,21). Chd contains a conserved Zn(II)-binding domain similar to enzymes in the metallo-β-lactamase superfamily and was proposed to be monomeric in solution (7). At least two His residues (H128 and H157) along with three Asp (D45, D130, and D184), a Ser (S126) and a Trp (W241) were reported to be essential catalytically based on site-directed mutagenesis studies. In addition, it was reported that the Zn(II) ions associated with Chd could be substituted with Cd(II), Co(II), Ca(II), or Mn(II) and provide active or even hyperactive enzymes (21). While the initial biological characterization of Chd has provided some insight into how molecular structure controls enzyme function, the mechanism of action remains entirely unknown.

Herein we report a new continuous spectrophotometric assay for Chd that has allowed the detection of a Chd reaction intermediate using UV-Vis stopped-flow spectroscopy with TPN as the substrate. From these stopped-flow data, along with metal binding and kinetic studies including pH and solvent isotope effect studies, we propose the first catalytic mechanism for Chd.

RESULTS

Protein Expression and Purification. The gene from pseudomanas sp. CTN-

3 that encodes for Chd was synthesized with optimized *E. coli* codon usage and includes a TEV protease cleavage site followed by a polyhistidine (His₆) affinity tag engineered onto the C-terminus. Expression of Chd and purification using immobilized metal affinity chromatography (IMAC) resulted in ~12 mg/L of soluble Chd enzyme. SDS gel page reveals a single polypeptide band at ~36 kDa (Supplemental Material Figure S1), consistent with previous studies (7,21). However, size exclusion chromatography indicates that Chd exists primarily as a dimer (~72 kDa) in solution in 50 mM HEPES buffer, pH 7.0, at 25 °C.

Spectrophotometric Enzymatic Assay. A continuous spectrophotometric enzymatic assay for Chd was developed by directly detecting 4-OH-chlorothalonil, the product of TPN hydrolysis by Chd, at 345 nm ($\varepsilon_{345} = 3.5 \text{ mM}^{-1}\text{cm}^{-1}$). This region contains no detectable substrate absorption (5). All kinetic data were recorded on a temperature-controlled Shimadzu UV-2450 spectrophotometer in 50 mM HEPES buffer, pH 7.0, at 25 °C, over a 60 s time period. Plots of the initial rate of hydrolysis of various concentrations of TPN were fit to the Michaelis-Menten equation, which provide a k_{cat} value of $24 \pm 2 \text{ s}^{-1}$ and a K_m value of $110 \pm 30 \text{ }\mu\text{M}$.

Metal Binding Properties of Chd. Apo-Chd was prepared by adding a 15 mM 1,10-Phenanthroline/40 mM EDTA solution to as-purified Chd under anaerobic conditions for ~24 h followed by desalting via column chromatography and dialysis against 50 mM HEPES, pH 7.0. The intrinsic dissociation constant (K_d) was determined by titrating apo-Chd at pH 7.0 in 50 mM HEPES buffer at 25 °C with Zn(II)_{aq} and monitoring the catalytic activity as a function of [Zn(II)]. K_d , and the number of binding sites, p, were determined by fitting these titration data to equation 1 (22), where r, the binding function, is defined by the fractionation saturation f_a and number of binding sites (equation 2) (23). In equation 1, C_s is the

$$r = p C_S / (K_d + C_S)$$
 (Eq. 1)

$$r = f_a p$$
 (Eq. 2)

concentration of free Zn(II). C_s was calculated from the total concentration of zinc added to the reaction (C_{TS}) by equation 3 (24), where C_A is the total molar concentration of enzyme (0.25 μ M).

$$C_{TS} = C_S + rC_A \tag{Eq. 3}$$

These data are plotted as r vs. [Zn(II)] (Figure 2). The best fits indicated a single Zn(II) binding site ($p = 1.03 \pm 0.01$) with an intrinsic $K_{\rm d}$ value of 0.17 ± 0.01 $\mu \rm M$. Attempts to fit these data with a cooperative model were inconclusive as the resulting goodness did not improve compared to the non-cooperative model. These data are consistent with inductively coupled atomic emission spectroscopy (ICP-AES) data obtained on as purified Chd, which revealed that ~ 0.9 equivalents of zinc bind tightly to Chd per monomer. No other first row transition metal ions were detected via ICP-MS (< 10 ppb).

pH Dependence of the Kinetic Parameters. The kinetic parameters $K_{\rm m}$, $k_{\rm cat}$, and $k_{\rm cat}/K_{\rm m}$ were determined as a function of pH using TPN as the substrate. Chd was found to exhibit a bell-shaped curve for plots of activity vs. pH over the pH range 4 to 10. The maximum catalytic activity occurred in the range of pH 6.5 to 9.2. Log($k_{\rm cat}$) and log($k_{\rm cat}/K_{\rm m}$) were fit to equations 4 and 5 (25),

$$\log k_{cat} = \log \left(\frac{k_{kcat}^{'}}{1 + 10^{pK_{ES1} - pH} + 10^{pH - pK_{ES2} - pH}} \right)$$
(Eq.4)

$$\log k_{cat}/K_{m} = \log \left(\frac{\left(\frac{K_{cat}}{K_{m}'}\right)}{1 + 10^{pK_{E1} - pH} + 10^{pH - pK_{E2}}} \zeta\right)$$
(Eq.5)

respectively, where: k'_{cat} is the theoretical maximal velocity; k'_{cat}/K'_{m} is the theoretical maximal catalytic efficiency; K_{ES1} is the ionization constant of the ES complex, which affects the acidic side of the pH curve while K_{ES2} reflects the basic side; and K_{E1} and K_{E2} are ionization constants for an acidic and basic group, respectively, on the free enzyme or free substrate. Inspection of a plot of $log(K_m)$ vs. pH (Figure 3) reveals that $K_{\rm m}$ exhibits a broad minimum over pH 5.5 to 7.5. A plot of $log(k_{cat})$ vs. pH provided a bellshaped curve that was fit to equation 4 (Figure 3) providing a p $K_{\rm ES1}$ value of 5.4 ± 0.2, a p $K_{\rm ES2}$ value of 9.9 ± 0.1 , and a k'_{cat} value of $24 \pm 2 \text{ s}^{-1}$. Similarly, plots of $log(k_{cat}/K_m)$ vs. pH were fit to equation 5 providing a p K_{E1} value of 5.4 \pm 0.3, a p K_{E2} value of 9.5 ± 0.1 , and a k'_{cat}/K'_{m} value of $220 \pm 10 \text{ s}^{-1}\text{mM}^{-1}$ (Figure 3).

Solvent Isotope Effect Studies. k_{cat} for TPN was measured, at several ratios of D₂O (${}^{2}H_{2}O$): ${}^{1}H_{2}O$ and the results are plotted in Figure 4 as atom fraction of

deuterium vs. V_n/V_0 , where V_n is the observed velocity at n fraction of deuterium and V_0 is the observed velocity in 100% $^1{\rm H}_2{\rm O}$. Proton inventories and fractionation factors were obtained by fitting the experimental values for V_n/V_0 to equations derived from the Gross-Butler equation (equation 6)(26), where v_n is the number

$$V_{n}/V_{0} = \frac{\prod_{j}^{v_{t}} (1 - n + n \phi_{i}^{T})}{\prod_{j}^{v_{R}} (1 - n + n \phi_{i}^{R})}$$
(Eq. 6)

of protons transferred in the transition-state, while υ_R is the number of protons transferred in the reactant state, and ϕ is the fractionation factor. Fitting revealed a linear relationship ($\upsilon_t = 1$, $\upsilon_R = 0$), indicating that one proton is transferred in the transition-state when $\phi_R = 1$ (equation 7) (27),

$$V_n = V_0 (1 - n + \phi_T n)$$
 (Eq.7)

where the experimental ϕ_T value is 0.17 while the theoretical value of ϕ_T is 0.18 (R² = 0.99) (Figure 4).

Calculation of the partial solvent isotope effect provides an alternative way to determine the number of protons transferred in the transition-state (28). At n = 0.5, the theoretical solvent isotope effect for a process involving N protons can be estimated using equation 8, a generalization of

$$V_{0.5}/V_1 = \left[(1 - n_{0.5}) (V_{0.5}/V_1)^{\frac{1}{N}} + n_{0.5} \right]^N$$
 (Eq.8)

equations 6 and 7 (29), where V_1 , V_0 , $V_{0.5}$ are the specific activities at 100% D₂O, 0% D₂O, and 50% D₂O, respectively. $V_{0.5}/V_1$ represents the

midpoint partial solvent isotope effect at 50% D_2O , while V_0/V_1 is the total isotope effect [(velocity in $100\%\ ^1\text{H}_2\text{O})$ \div (velocity in $100\%\ D_2O$)]. The experimental midpoint partial isotope effect was 2.98 and the calculated midpoint partial isotope effect for a one proton transfer (Equation 8) was found to be 2.99 (Table 1). For comparison purposes, the midpoint partial isotope effect calculated for a two-proton transfer in the transition-state is 4.03.

Stopped-flow experiments. Steady-state kinetic data were obtained using a 0.25 mM buffered solution of [TPN] at pH 7.0 and 4 °C. Because of the

observed decrease in $k_{\rm cat}$ at lower pH values, stopped-flow spectrophotometric data were also collected at 4 °C and pH 5.0, however, the reaction still remained too fast to obtain pre-steady-state kinetic data. However, when stopped-flow experiments were performed in 99% D₂O in 50 mM acetate buffer at pH 5.0 and 4 °C with 250 μ M TPN, a burst of absorbance was observed (Figure 5) that could be modeled using a two-component expression containing linear and exponential terms (equation 9) (30,31), where [P]

$$\frac{[P]}{[E]} = A_0 (1 - e^{k_{obs}t}) + k_{cat}t$$
 (Eq. 9)

is the product concentration, [E] is the enzyme concentration, A_0 is the burst amplitude, k_{obs} is the overall rate constant, and k_{cat} is the turnover number ($R^2 = 0.98$). As this experiment is performed under saturating substrate concentrations, k_1 ' for formation of the Michaelis complex is large. Therefore, it does not influence the multiple turnover kinetics and theoretical modeling of the data returns information only on the formation of a post-Michaelis intermediate k_2 and product release k_3 (equations 10 and 11).

$$A_0 = \mathcal{L}$$
 (Eq. 10)
 $k_{obs} = k'_2 + k'_3$ (Eq. 11)

(Table 2) (30). Fits of these data (Figure 5) provided apparent rate constants k_2 of $35.2 \pm 0.1 \text{ s}^{-1}$, and k_3 of $1.1 \pm 0.2 \text{ s}^{-1}$. The k_{cat} of the overall reaction was calculated to be $1.1 \pm 0.1 \text{ s}^{-1}$ in good agreement with the value calculated using equation 12, which provided a k_{cat} value of $1.08 \pm 0.02 \text{ s}^{-1}$.

$$k_{cat} = \frac{k'_2 k'_3}{k'_2 + k'_3}$$
 (Eq.12)

These data were compared to experimentally determined steady-state kinetic data obtained at 4 °C for Chd using 250 μ M TPN as the substrate at pH 5.0 in 99% D₂O acetate buffer. Under these conditions, $k_{\text{cat}} = 1.08 \pm 0.01 \text{ s}^{-1}$ and $K_{\text{m}} = 71 \pm 3 \mu$ M (Table 2).

DISCUSSION

The prevailing dogma is that biological dechlorination reactions are catalyzed by oxidative, reductive, or thiolytic dehalogenation processes (9-15). A relatively unknown biological dehalogenation

process involves hydrolysis of a C-Cl bond (32). Chd, a Zn(II)-dependent enzyme, has been shown to catalyze the hydrolytic dehalogenation of TPN to 4-OH-TPN and chloride (Scheme 1) under ambient conditions (7,21). As Chd can hydrolyze an aromatic C-Cl bond, understanding the inorganic and biological chemistry of Chd will provide insight into its catalytic mechanism, which in turn will the assist in the development of biocatalysts or small biomimetic catalysts that can be used in the environmental clean-up of TPN. To date, no catalytic mechanism has been proposed for Chd, in part because of the lack of an enzymatic assay that allows for the direct detection of product, which has prevented detailed kinetic studies.

To overcome this obstacle, a spectrophotometric kinetic assay was developed that directly detects the formation of 4-OH-chlorothalonil at 345 nm, a wavelength where there is little or no TPN absorbance (5). Initial control reactions were performed with saturating amounts of TPN (250 µM) in 50 mM HEPES buffer at pH 7 and 25 °C in the absence of Chd by monitoring absorptions between 300 and 400 nm to determine if any TPN hydrolysis occurred under the experimental conditions used. The addition of 1 µM Zn(II) to these reaction mixtures also produced no detectable absorption at 345 nm. With no increase in absorbance observed, Chd was added to a final concentration of 10 µM resulting in a steady increase in absorption at 345 nm. The rate of increase at 345 nm was highly reproducible and dependent on the concentration of Chd and TPN as well as the temperature and pH of the reaction mixture. temperatures above 30 °C gradual inactivation occurs, which is indicative of Chd denaturation. established the viability of directly detecting the product of TPN hydrolysis, the kinetic parameters k_{cat} and $K_{\rm m}$ were determined at pH 7.0 and 25 °C over a 60 s time period. Plots of [TPN] vs initial rate were fit to the Michaelis-Menten equation, which provided a k_{cat} value of 24 \pm 2 s⁻¹ and a K_{m} value of 110 \pm 30 uM, in good agreement with values previous reported using a non-continuous HPLC based assay performed under similar reaction conditions (7,21).

The development of a continuous spectrophotometric assay for Chd; has allowed us to ask and answer several basic biological and mechanistic questions, such as: How many active site metal ions are required for full enzymatic activity? How many ionizable groups are required for catalysis? How many protons are transferred in the

transition-state? and, what is the rate-limiting step in the reaction? It has been suggested that Chd requires two Zn(II) ions to be fully active and that these Zn(II) ions form a dinuclear active site (7,21). However, inductively coupled atomic emission spectroscopy (ICP-AES) data obtained on as-purified Chd revealed that ~0.9 Zn(II) ions bind per monomer and size exclusion chromatography indicates that Chd exists primarily as a dimer (~72 kDa) in solution.

Activity titrations indicated that maximum catalytic activity is observed with only one Zn(II) ion per monomer of Chd with an intrinsic $K_{\rm d}$ value of 0.17 μ M, suggesting that any other Zn(II) binding is unrelated to catalysis. It should be noted that in previous studies, the His₆-tag was not removed before kinetic data were obtained (7,21). As His₆-tags have high affinity for Zn(II) ions (33), it is possible that adventitious metal binding to the His₆-tag led to the suggestion that more than one metal ion is required for catalysis.

Quantitative analysis of the pH-dependence of Chd activity suggested [c.f.(34)] that one catalytically competent ionizable group with $pK_{ES1} \approx 5.4$ must be deprotonated in the ES complex, and another with $pK_{ES2} \approx 9.9$ must be protonated, respectively, to facilitate catalysis. Assignment of the observed p $K_{\rm ES}$ values is difficult in the absence of an X-ray crystal structure; however likely candidates for p K_{ES1} are the deprotonation of an active site His residue (35) (whose putative pK_a is 5-7 (36)) or an Asp/Glu residue, while p $K_{\rm ES2}$ might be due to the deprotonation of the leaving group or an active site residue such as an Arg or Lys (7). Alternatively, pK_{ES2} may be due to the deprotonation of a Ser residue that which was shown to be required for catalysis (7) or a metalbound water molecule depending on which catalytic mechanism is operable.

Analysis of the pH-dependence of $\log(k_{\rm cat}/K_{\rm m})$ [c.f. (35)] provided a p $K_{\rm E1}$ value of 5.4 and a p $K_{\rm E2}$ value of 9.5 for two enzyme-centered ionizable groups, respectively, that are involved in catalysis. p $K_{\rm E1}$ is most likely due to an active site His or an Asp/Glu residue but could also be the deprotonation of the metal-coordinated water molecule. Moreover, the enzyme-centered p $K_{\rm E2}$ value, like p $K_{\rm ES2}$, is most likely due to the deprotonation of an active site residue such as an Arg or Lys but could also be deprotonation of the metal bound water molecule.

Kinetic isotope effect studies are an excellent way to gain an understanding of the nature of the ratelimiting step as well as probe the transition-state of catalytic reactions (37). Primary isotope effects are observed if a bond to the labeled atom is made or broken during the reaction whereas secondary isotope effects describe processes at other positions. We examined the ¹H/²H solvent isotope effect of Chd using TPN as the substrate at pH 7.0, $(p^2H = p^1H)$ meter reading + 0.4) (38). The intrinsic primary isotope effect, $k_{\rm H}/k_{\rm D}$, is related to the symmetry of the transition-state for that step (i.e. the larger the isotope effect, the more symmetrical the transition-state) with the theoretical limit being 9 at 37°C in the absence of tunneling effects. For the simplest case, in which a single proton produces the solvent isotope effect, a plot of atom fraction of deuterium vs. V_n/V_0 is linear, where V_n is k_{cat} at a particular fraction of deuterium and V_0 is k_{cat} in buffer containing 0% D₂O (39). The presence of D₂O lowers the catalytic activity of Chd and results in a solvent isotope effect of 2.98. This normal isotope effect suggests that an O-H bond is broken in the transition-state.

For Chd, V_n/V_0 is a linear function of n indicating that one proton is transferred during catalysis with a fractionation factor of 0.17. Analysis of the midpoint solvent isotope effect also supports involvement of a single proton transferred in the transition-state. Therefore, the Zn(II) ions appear to be responsible for the proper positioning of the hydroxyl group relative to the substrate and this hydroxyl group likely interacts with a general base, such an His or Asp/Glu residue. Based on these data and the observed $pK_{\rm El}$ and $pK_{\rm ES2}$ values, a His residue appears most likely to facilitate the transfer of a proton and likely reflects the transfer of a proton from an active site water molecule to an active site His residue forming a more nucleophilic hydroxide.

Based on these data, the simplest model was used that describes the observed changes in ionization states of active site residues with changing pH and the number of protons transferred in the transition-state (Scheme 2). This model **Scheme 2.** Proposed kinetic model for Chd where E(H₂O) is enzyme containing water molecule at active site, E^P is the enzyme at protonated, E^D is the enzyme at deprotonated, S represents substrate, ES(H₂O) represent the enzyme-substrate complex containing water molecule at active site, E^PS is the enzyme-substrate complex at protonated state, E^DS is the enzyme-substrate comple at deprotonated state, [I] is an intermediate state with deprotonated water and [P] is product.

$$E^{P} \qquad E^{P}S$$

$$\downarrow k_{E1} \qquad \downarrow k_{ES1} \qquad k_{2}$$

$$E(H_{2}O) + S \qquad k_{1} \qquad ES(H_{2}O) \xrightarrow{k_{2}} I(OH) \xrightarrow{k_{3}} E(H_{2}O) + P$$

$$\downarrow k_{E2} \qquad \downarrow k_{ES2}$$

$$E^{D} \qquad E^{D}S$$

assumes that: i) the substrate-binding step leading to the formation of an enzyme-substrate complex following steady-state kinetics (*e.g.* the enzyme, substrate and enzyme-substrate complex are at equilibrium) and k_{-1} is larger than k_{2} as neither the substrate or the product are sticky and $k_{2}+k_{3}$ contains the rate-limiting step (*i.e.* C-Cl bond breaking or product release). Since there is no clear absorption change as [ES] and intermediate signal within the burst phase, we assume k_{2} and k_{3} are irreversible (30,31).

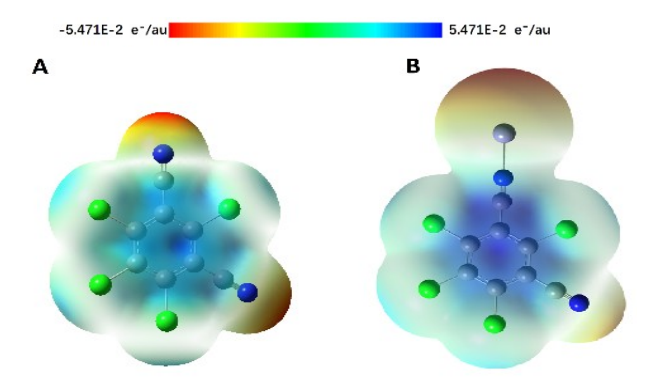
An important question in understanding the hydrolysis of TPN by Chd is: "What is the rate-limiting step in the catalytic reaction?" Pre-steady-state kinetic data indicated that formation of the Michaelis complex is very fast compared to the hydrolysis and product-release steps and, therefore, the rate constants for the latter two could be estimated from multiple-turnover stopped-flow spectrophotometry. Based on these data, a minimal three-step kinetic model is proposed that allows for fast reversible substrate binding, the formation of a post-Michaelis pre-transition-state intermediate, and the post-transition-state release of product (Scheme 3).

Scheme 3. Proposed pre-steady state model for the dechlorination of TPN by Chd.

$$E(H_2O) + S \xrightarrow{k_1} ES(H_2O) \xrightarrow{k_2} I(OH) \xrightarrow{k_3} E(H_2O) + P$$

The electron density distribution of free and Zn(II) bound TPN calculated using Gaussian 9-win (Scheme 4), and the previously reported kinetic and site-directed mutagenesis data (7,21), suggests two possible catalytic mechanisms for the

Scheme 4. Gaussian-9 derived electron density map of TPN (A) and TPN bound to a Zn(II) ion (B). (carbon: gray; nitrogen: blue; chlorine: green; zinc: dark gray).



hydrolysis of TPN by Chd (Figure 6). We propose the initial catalytic step involves the binding of the nitrile nitrogen, to the active site Zn(II) ion, which results in the removal of electron density from the aromatic ring activating the ortho carbon for nucleophilic attack (Scheme 4; B) (40,41). The significantly enhanced electrophilic character of the ortho carbon upon nitrile binding to Zn(II) suggests that Zn(II) binding activates the ortho carbon towards nucleophilic attack and may also help to position the ortho carbon relative to the nucleophile, thus preorganizing the transition-state. Based on our kinetic data, an active site His residue needs to be deprotonated so it can accept a single proton from a Zn(II)-bound water molecule providing the catalytic nucleophile, which is pre-organized adjacent to the activated ortho carbon of TPN. Once nucleophilic attack occurs, Cl- and 4-OH-TPN are formed and released from the active site, which is the ratelimiting step in catalysis. Finally, a water molecule binds to the active site Zn(II) thus reforming the active catalyst.

Even though the mechanistic proposal involving nitrile binding to the active site Zn(II) ion is logical and has advantages in that binding activates the ortho carbon for nucleophilic attack and pre-organizes the transition-state by positioning the Zn(II) bound hydroxide near the ortho carbon, there is no experimental evidence to support TPN binding to the active site Zn(II) ion at this time. Therefore, an alternative pathway involving substrate binding near

the active site but not directly to the Zn(II) ion, must also be considered (Figure 6B). Under such a scenario, a protonated active site residue (R₁) would form a hydrogen bond with the nitrile nitrogen. Previous studies as well as our pH dependent assay suggest an active site Ser or Trp might play such as both were found to be essential for catalysis. The existence of an R1 residue is supported by the loss of catalytic activity at high pH values. Moreover, the electron density map of TPN in the absence of nitrile Zn(II) binding reveals some electrophilic character at the ortho carbon (Scheme 4; A), suggesting susceptibility to nucleophilic attack. This active site residue would pre-organize the ortho carbon with the Zn(II)-bound hydroxide nucleophile, which like in pathway A would transfer a proton to the active site acid/base His residue in the transition-state. Once nucleophilic attack occurs, like pathway A, Cl⁻ and 4-OH-TPN are formed and released from the active site. which is the rate-limiting step in catalysis. A water molecule would then bind to the active site Zn(II), reforming the active catalyst.

In conclusion, the development of a continuous spectrophotometric assay that allows for the direct detection of the product 4-OH-TPN, has allowed the first mechanistic studies to be carried out on the hydrolytic dehalogenase, Chd. Metal titration data indicate that a single metal ion is required for catalytic activity so Chd can be classified as a mononuclear hydrolytic Zn(II)-dependent enzyme. Chd is a dimer in solution and exhibits a broad kinetic pH dependence with the maximum velocity dependent on two ionizable groups, one with $pK_a \approx$ 5.4 and one with a p $K_a \approx 9.9$. Solvent kinetic isotope effect studies indicate that one proton is transferred in the transition-state, likely due to the breaking of a water O-H bond. Pre-steady state kinetic studies performed under saturating substrate conditions revealed a burst phase followed by a linear, steadystate phase. Determination of k_2 and k_3 revealed that the product release step is the slow-step in the catalytic cycle. Taken together, along with density functional calculations on TPN in the absence and presence of Zn(II), have allowed two potential catalytic mechanisms to be proposed. Further studies will be required to distinguish between mechanistic pathways A or B.

EXPERIMENTAL PROCEDURES

Materials. Synthesized genes and primers were purchased from Genscript (Piscataway, NJ 08854). All other chemicals were purchased from commercial sources and were of the highest quality available

Pseudomonas sp. CTN-3 TPN dehalogenase (Chd) plasmid construction. Chd sequences were obtained by BLAST search using Uniprot (Uniport ID: C9EBR5). Proposed active site motifs for Chd were identified based on the metallo-β-lactamase superfamily. The predicted gene was synthesized with optimized *E. coli* codon usage by Genscript Inc (Piscataway, NJ 08854). A polyhistidine (His6) affinity tag was engineered onto the C-terminus with a TEV cleavage site using Phusion DNA polymerase (New England Biolabs) and subcloned into a pET28a⁺ (EMD Biosciences) expression vector. The sequence was confirmed using automated DNA sequencing at Functional Biosciences (Madison, WI).

Expression and Purification of Chd. The Chd plasmid was freshly transformed into BL21(DE3) competent cells (Stratagene), and a single colony was used to inoculate 50 ml of LB-Miller culture containing 50 µg/mL kanamycin with shaking overnight at 37 °C. This culture was used to inoculate a 1 L culture and the cells were grown at 37 °C until the OD_{600nm} reached 0.8-1.0. The culture was cooled on ice, induced with 0.1 mM isopropyl β-D-1thiogalactopyranoside (IPTG) supplemented with 0.05 mM ZnCl₂, and expressed at 25 °C for 16 hours. Cells were harvested by centrifugation at 6370 x g and 4 °C for 10 min in a Beckman Coulter Avanti JA-10 rotor. Cell pellets were resuspended in 20 mM Tris-HCl buffer containing 50 mM NaCl and 25 mM imidazole at a ratio of 5 ml per gram of cells, then sonicated for 4 min (30 s on 45 s off) at 21W using a Misonix sonicator 3000. The crude extract was obtained after centrifugation in a JA-20 rotor at 31,000 x g and 4 °C for 20 min.

Crude extracts of Chd (100 mg) were loaded onto a 5 ml Ni-NTA (nitrilotriacetic acid) Superflow Cartridge (Qiagen) for immobilized metal affinity chromatography (IMAC) using an ÄKTA FPLC P-960. The column was washed with 50 mL of 20 mM Tris-HCl buffer containing 50 mM NaCl and 25 mM imidazole, followed by 50 mL of 20 mM Tris-HCl buffer containing 50 mM NaCl and 75 mM imidazole. The protein was eluted using a linear imidazole gradient (75 to 500 mM) at a flow rate of 2 mL/min.

Active protein fractions were pooled and concentrated using 50 mM Tris buffer containing 1 mM EDTA with an Amicon Ultra-15 10,000 MWCO centrifugal filter unit (Millipore) resulting in ~12 mg/L of soluble Chd-His₆.

The His₆-tag was removed by treating His₆-tagged Chd with His6-tagged TEV protease (EC 3.4.22.44) for 16 h at 4 °C in 50 mM Tris, pH 8.0. Cleaved protein was concentrated with a Centricon (15,000-MW cutoff; Amicon) to 3 mL and loaded on IMAC to remove the remaining cleaved His6-tag, uncut protein and the His6-tagged TEV protease, while the flow through containing Chd was collected and washed with 50 mM HEPES buffer containing 10% glycerol at pH 7.0. Purified protein samples were analyzed by SDS-PAGE with a 12.5% polyacrylamide SPRINT NEXT GELTM (Amresco). Gels were stained with Gel Code Blue (Thermo-Fisher Scientific). Protein concentration of crude extracts was determined using a Coomassie (Bradford) Protein Assay Kit (Pierce) and of pure protein by measuring the absorbance at 280 nm with a Shimadzu UV-2450 spectrophotometer equipped with a TCC-240A temperature-controlled cell holder. Theoretical molecular weights and protein extinction coefficients were calculated with the ExPASy compute pI/Mw tool. The molecular weight for Chd was 36,107 g/mol with an extinction coefficient of 42,525 cm⁻¹ M⁻¹. This molecular weight is in good agreement with SDS-PAGE data.

Chd Spectrophotometric Assay. The enzymatic activity of Chd towards TPN was measured using a Shimadzu UV-2450 spectrophotometer equipped with a TCC-240A temperature-controlled cell holder in 1 mL quartz cuvettes. A 1 mL reaction consisted of 50 mM HEPES buffer, 0.01µM Chd, pH 7.0 at 25 °C and various concentrations of TPN up to 250 µM. The rate of TPN dehalogenation was determined by continuously monitoring the formation of 4-OH-TPN at 345 nm ($\Delta \varepsilon_{345} = 3.5 \text{ mM}^{-1}\text{cm}^{-1}$) (5). Data analysis was performed using OriginPro 9.0 (OriginLab, Northampton, MA). The kinetic constants V_{max} and $K_{\rm m}$ were calculated by fitting these data to the Michaelis-Menten equation. $V_{\rm max}$ values were converted to k_{cat} using the molar mass of Chd. One unit of enzyme activity was defined as the amount of enzyme that catalyzed the production of 1 µmol of TPN per minute at 25 °C.

Metal Analysis. As_-purified enzyme samples of Chd were digested with concentrated nitric acid at 70 °C for 10 minutes and then cooled to room

temperature. These samples were diluted to 5 ml total volume with deionized water to give a final nitric acid concentration of 5% and were filtered using 0.2 μ m Supor membrane syringe filters (Pall). A nitric acid blank was also prepared. The samples were analyzed using inductively coupled atomic emission spectroscopy (ICP-AES) at the Water Quality Center in the College of Engineering at Marquette University (Milwaukee, WI, USA).

 K_d Apo-Enzyme Preparation and Zn(II)Determination. Apo-Chd was obtained by incubating as-purified enzyme in 15 mM a Pphenanthroline/40 mM EDTA solution under anaerobic conditions for ~24h. The metal chelators were removed via a PD-Minitrap G10 desalting column followed by dialysis using a Slide-A-Lyzer dialysis cassette for 16 h with Chelex 100 treated 50 mM HEPES at pH 7.0. Titration of Zn(II) into apo-Chd was performed on a Shimadzu UV-2450 spectrophotometer equipped with a TCC-240A temperature-controlled cell holder in 1 mL quartz cuvettes in 50 mM HEPES buffer, 0.25 µM of apo-Chd, pH 7.0 at 25 °C. The rate of hydrolysis of TPN (0.25 mM) was monitored as a function of [Zn(II)].

pH Profiles. The enzymatic activity of 0.01 μM Chd at pH values between 4.0 and 10.2 were measured using TPN as the substrate. The concentration of each buffer used was 50 mM and the following buffers were used: borate (pH 8.50-10.50); Tris HCl (pH 7.00-8.50); HEPES (pH 6.8-7.2); MOPS (pH 6.50-7.00); MES (pH 5.50-6.50); acetate (pH 3.23-5.50). The kinetic parameters k_{cat} , K_m and k_{cat}/K_m , were determined using

8-12 different substrate concentrations ranging from 0.2-2.5 times the observed $K_{\rm m}$ value at each pH studied. Kinetic parameters and fits to the kinetic curves were obtained using OriginPro 9.0 (OriginLab, Northampton, MA).

Solvent Isotope effect. All buffers were prepared from freshly opened bottles of 99.9% [²H] H₂O and CH₃OH (Aldrich). The buffers used in the preparation of all deuterated buffers were in the anhydrous form. The pD of each buffer used was adjusted by the addition of NaOD or DCl (both 99%+ deuterium content; Acros Organics, Geel, Belgium) and corrected for deuteration by adding 0.4 to the reading of the pH electrode (28).

Stopped-flow experiments. Chd activity towards TPN was examined in triplicate using a single mixing Applied Photophysics SX-20 stopped-flow UV-vis spectrophotometer with a 20 μ m cell. Chd activity was monitored at 345 nm by acquiring stopped-flow data from 0.005 to 1 second at 4 °C using 8.1 μ M enzyme and 250 μ M TPN in deuterated 50 mM acetate buffer pH 5.0. All data were fit using OriginPro 9.0 (OriginLab, Northampton, MA).

TPN Electron Density Calculation. The structures of TPN were drawn using Gaussian View 5.0.8. The bond lengths and overall structures were optimized by DFT calculations at the ground state (basis set: 3-21G) followed by electron density distribution of free TPN by Gaussian 9-win.

Acknowledgments: We thank the National Science Foundation (CHE-1808711, RCH & BB) for funding this research.

Conflict of interest: The authors declare that they have no conflicts of interest with the contents of this article.

Author contributions: XY prepared expression plasmid, carried out protein expression, purification, enzymatic assays and stopped-flow experiments, prepared samples for metal analysis, and analyzed the results. RCH and BB conceived of the idea and wrote the paper with XY.

References

- 1. Caux, P. Y., Kent, R. A., Fan, G. T., and Stephenson G. L. (1996) Environmental fate and effects of chlorothalonil: A Canadian perspective *Crit. Rev. Environ. Sci. Technol.* **26**, 45-93
- 2. Sakkas, V. A., Lambropoulou, D. A., and Albanis, T. A. (2002) Study of chlorothalonil photodegradation in natural waters and in the presence of humic substances. *Chemosphere* **48**, 939-945
- 3. Mozzachio, A. M., Rusiecki, J. A., Hoppin, J. A., Mahajan, R., Patel, R., Beane-Freeman, L., and Alavanja, M. C. (2008) Chlorothalonil exposure and cancer incidence among pesticide applicator participants in the agricultural health study. *Environmental research* **108**, 400-403
- 4. Carlo-Rojas, Z., Bello-Mendoza, R., Figueroa, M. S., and Sokolov, M. (2004) Chlorothalonil Degradation under Anaerobic Conditions in an Agricultural Tropical Soil. *Water, Air, & Soil Pollution* **151**, 397-409
- 5. Kwon, J. W., and Armbrust, K. L. (2006) Degradation of chlorothalonil in irradiated water/sediment systems. *Journal of agricultural and food chemistry* **54**, 3651-3657
- 6. Vickers, A., Sloop, T., and Lucier, G. (1985) Mechanism of Action of Toxic Halogenated Aromatics. *Environ Health Perspect.* **59**, 121-126
- 7. Wang, G., Li, R., Li, S., and Jiang, J. (2010) A Novel Hydrolytic Dehalogenase for the Chlorinated Aromatic Compound Chlorothalonil. *J. Bacteriol.* **192**, 2737–2745
- 8. Viciu, M. S., Grasa, G. A., and Nolan, S. P. (2001) Catalytic Dehalogenation of Aryl Halides Mediated by a Palladium/Imidazolium Salt System. *Organometallics* **20**, 3607-3612
- 9. Reddy, G. V., and Gold, M. H. (2000) Degradation of pentachlorophenol by Phanerochaete chrysosporium: intermediates and reactions involved. *Microbiology* **146** (**Pt 2**), 405-413
- 10. Beil, S., Mason, J. R., Timmis, K. N., and Pieper, D. H. (1998) Identification of chlorobenzene dioxygenase sequence elements involved in dechlorination of 1,2,4,5-tetrachlorobenzene. *Journal of bacteriology* **180**, 5520-5528
- 11. Xun, L., Topp, E., and Orser, C. S. (1992) Purification and characterization of a tetrachloro-phydroquinone reductive dehalogenase from a Flavobacterium sp. *Journal of bacteriology* **174**, 8003-8007
- 12. Orser, C. S., Dutton, J., Lange, C., Jablonski, P., Xun, L., and Hargis, M. (1993) Characterization of a Flavobacterium glutathione S-transferase gene involved reductive dechlorination. *Journal of bacteriology* **175**, 2640-2644
- 13. Yokota, T., Fuse, H., Omori, T., and Minora, Y. (1986) Microbial dehalogenation of haloalkanes mediated byoxy genases or halidohydrolase. *Agric. Biol. Chem.* **50**, 453–460
- 14. Leisinger, T., Bader, R., Hermann, R., Schmid-Appert, M., and Vuilleumier, S. (1994) Microbes, enzymes and genes involved in dichloromethane utilization. *Biodegradation* **5**, 237-248
- 15. Bunge, M., ., Adrian, L., Kraus, A., Opel, M., Lorenz, W. G., Andreesen, J. R., Görisch, H., and Lechner, U. (2003) Reductive dehalogenation of chlorinated dioxins by an anaerobic bacterium. *Nature* **421**, 357-360
- 16. van der Ploeg, J., van Hall, G., and Janssen, D. B. (1991) Characterization of the haloacid dehalogenase from Xanthobacter autotrophicus GJ10 and sequencing of the dhlB gene. *Journal of bacteriology* **173**, 7925-7933
- 17. Verschueren, K. H., Seljée, F., Rozeboom, H. J., Kalk, K. H., and Dijkstra, B. W. (1993) Crystallographic analysis of the catalytic mechanism of haloalkane dehalogenase. *Nature* **363**, 693-698
- 18. Liang, B., Wang, G., Zhao, Y., Chen, K., Li, S., and Jiang, J. (2011) Facilitation of bacterial adaptation to chlorothalonil-contaminated sites by horizontal transfer of the chlorothalonil hydrolytic dehalogenase gene. *Applied and environmental microbiology* 77, 4268-4272
- 19. Ren, X., Li, H., and Chen, S. (2011) Cloning of the chlorothalonil-degrading gene cluster and evidence of its horizontal transfer. *Current microbiology* **62**, 1068-1073

- 20. Yue, W., Xiong, M., Li, F., and Wang, G. (2015) The isolation and characterization of the novel chlorothalonil-degrading strain Paracoccus sp. XF-3 and the cloning of the chd gene. *Journal of bioscience and bioengineering* **120**, 544-548
- 21. Chen, H., Wang, H., Wang, T., Huang, S., Zang, X., Li, S., and Jiang, J. (2016) Identification of the metal center of chlorothalonil hydrolytic dehalogenase and enhancement of catalytic efficiency by directed evolution. *Applied Environmental Biotechnology* 1, 30-37
- 22. D'Souza V, M., Bennett, B., Copik, A. J., and Holz, R. C. (2000) Divalent metal binding properties of the methionyl aminopeptidase from Escherichia coli. *Biochemistry* **39**, 3817-3826
- Winzor, D. J., and Sawyer, W. H. (1995) *Quantitative characterization of ligand binding*, New York: Wiley-Liss, c1995.
- 24. Watterson, S. J., Mitra, S., Swierczek, S. I., Bennett, B., and Holz, R. C. (2008) Kinetic and spectroscopic analysis of the catalytic role of H79 in the methionine aminopeptidase from Escherichia coli. *Biochemistry* 47, 11885-11893
- 25. Dreyton, C. J., Knuckley, B., Jones, J. E., Lewallen, D. M., and Thompson, P. R. (2014) Mechanistic studies of protein arginine deiminase 2: evidence for a substrate-assisted mechanism. *Biochemistry* **53**, 4426-4433
- 26. Anderson, V. E. (1992) Isotope effects on enzyme-catalyzed reactions. *Current Opinion in Structural Biology* **2**, 757-764
- 27. Jenson, D. L., and Barry, B. A. (2009) Proton-coupled electron transfer in photosystem II: proton inventory of a redox active tyrosine. *J Am Chem Soc* **131**, 10567-10573
- 28. Mitra, S., and Holz, R. C. (2007) Unraveling the catalytic mechanism of nitrile hydratases. *The Journal of biological chemistry* **282**, 7397-7404
- 29. Elrod, J. P., Hogg, J. L., Quinn, D. M., Venkatasubban, K. S., and Schowen, R. L. (1980) Protonic reorganization and substrate structure in catalysis by serine proteases. *J Am Chem Soc* **102**, 3917-3922
- 30. Chow, C., Xu, H., and Blanchard, J. S. (2013) Kinetic characterization of hydrolysis of nitrocefin, cefoxitin, and meropenem by beta-lactamase from Mycobacterium tuberculosis. *Biochemistry* **52**, 4097-4104
- 31. Biro, F. N., Zhai, J., Doucette, C. W., and Hingorani, M. M. (2010) Application of stopped-flow kinetics methods to investigate the mechanism of action of a DNA repair protein. *Journal of visualized experiments : JoVE*
- 32. Ang, T. F., Maiangwa, J., Salleh, A. B., Normi, Y. M., and Leow, T. C. (2018) Dehalogenases: From Improved Performance to Potential Microbial Dehalogenation Applications. *Molecules* **23**
- 33. Evers, T. H., Appelhof, M. A., Meijer, E. W., and Merkx, M. (2008) His-tags as Zn(II) binding motifs in a protein-based fluorescent sensor. *Protein Eng Des Sel* **21**, 529-536
- 34. Cleland, W. W. (1997) Mechanisms of enzyme-catalyzed reactions. *Advances in Enzymology and Related Areas of Molecular Biology* **45**, 273-387
- 35. Hubert Bradford Vickery, C. S. L. (1928) ON THE SEPARATION OF HISTIDINE AND ARGININE. *Journal of biological chemistry* **78**, 627-635
- 36. Dey, A., Chow, M., Taniguchi, K., Lugo-Mas, P., Davin, S., Maeda, M., Kovacs, J. A., Odaka, M., Hodgson, K. O., Hedman, B., and Solomon, E. I. (2006) Sulfur K-Edge XAS and DFT Calculations on Nitrile Hydratase: Geometric and Electronic Structure of the Non-heme Iron Active Site. *J. Am. Chem. Soc.* 128, 533 541
- 37. Cleland, W. W. (1982) Use of isotope effects to elucidate enzyme mechanisms. *Crit. Rev. Biochem.* **13**, 385-427
- 38. Salomaa, P., Schaleger, L. L., and Long, F. A. (1964) Solvent Deuterium Isotope Effects on Acid-Base Equilibria. *J. Am. Chem. Soc.* **86**, 1-7
- 39. Elrod, J. P., Hogg, J. L., Quinn, D. M., Venkatasubban, K. S., and Schowen, R. L. (1980) Protionic reorganization and substrate structure in catalysis by serine proteases. *J. Am. Chem. Soc.* **102**, 3917-3922

- 40. Martinez, S., Wu, R., Sanishvili, R., Liu, D., and Holz, R. (2014) The active site sulfenic acid ligand in nitrile hydratases can function as a nucleophile. *J Am Chem Soc* **136**, 1186-1189
- 41. Light, K. M., Yamanaka, Y., Odaka, M., and Solomon, E. I. (2015) Spectroscopic and Computational Studies of Nitrile Hydratase: Insights into Geometric and Electronic Structure and the Mechanism of Amide Synthesis. *Chem Sci* 6, 6280-6294

FOOTNOTES

The abbreviations used are: TPN, chlorothalonil; Chd, TPN dehalogeanse; ORF, open reading frame; inductively-coupled plasma mass spectrometry; ICP-MS; IMAC, immobilized metal affinity chromatography.

 Table 1. Kinetic Parameters from solvent isotope study.

| | Experimental | One proton | Two protons | General solvation | |
|----------------------------------|--------------|--------------|--------------|-------------------|--|
| | value | (Calculated) | (Calculated) | (Calculated) | |
| V _{0.5} /V ₁ | 2.98 | 2.99 | 4.03 | 2.34 | |

 Table 2. Kinetic Parameters from stopped-flow experiment

| | A_0 | K _{obs} /s | k_{cat} (fitting) | k ₂ '/s | k' ₂ /s | k_{cat}/s (observed) |
|----------------|-------|---------------------|---------------------|--------------------|--------------------|------------------------|
| Value | 0.93 | 36.34 | 1.08 | 35.20 | 1.13 | 1.10 |
| Standard error | 0.01 | 0.29 | 0.01 | 0.10 | 0.19 | 0.06 |

Figure Captions

Figure 1. Chd sequence alignments for nine bacterial species. Yellow: proposed active site motif.

Figure 2. Zn(II) titration into apo-Chd (10 μ M). Each data point was obtained in triplicate in 50 mM HEPES buffer, pH 7.0 at 25 °C and 0.25 mM chlorothalonil. Fits by equation 1 provided a p value of ~1 and a K_d value of 0.17 \pm 0.01 μ M

Figure 3. pH dependence of the kinetic parameters for dechlorination of TPN by Chd between pH 4.0 and 10.0. Each data point was obtained in triplicate in 50 mM borate (pH 8.50-10.50); Tris HCl (pH 7.00-8.50); HEPES (pH 6.8-7.2); MOPS (pH 6.50-7.00); MES (pH 5.50-6.50); acetate (pH 3.23-5.50) at 25 °C and 0.25 mM chlorothalonil. The pH dependence of $\log k_{cat}$ was fit by equation 2 while the pH dependence of $\log k_{cat}/K_m$ was fit by equation 3. A plot of pH vs $\log K_m$ exhibited "V" shape curve that was fit with a polynomial equation. Error bars were smaller than the symbols used.

Figure 4. Plot of V_n/V_0 vs. atom fraction of deuterium for Chd at pH 7.0. Each data point was obtained in triplicate in 50 mM HEPES buffer under various ratios of D₂O/H₂O at 25 °C and 0.25 mM TPN. Solid line: data fit by a linear equation; Dashed line: direct fit to Equation 4 with fractionation ϕ_R =1, ϕ_T =0.18. Error bars were smaller than the symbols used.

Figure 5. Stopped-flow experiment data obtained by 50 mM acetate in 99% D_2O at 4°C, pD = 5.0. These data were fit (solid line) as an exponential for the pre-steady state burst phase and with a linear equation for the steady-state region.

Figure 6. Proposed catalytic mechanisms for Chd. Pathway A: An active site base acts as a proton acceptor for a Zn(II)-bound water. The Cl⁻ at the ortho carbon position is substituted by nucleophilic

attack of OH⁻. Pathway B: TPN is stabilized by a hydrogen bonding interactions with a protonated active site residue (R₁).

Figure 1

```
Rhodococus sp. XF-6 ------MPPGCSGLCSFVGLTMPLKFSGVLCASLLTITLSVAAHATELILDFNKVQMRSQQLAPGV 60
Rhodococus sp. XF-3 -------MPPGCSGLCSFVGLTMPLKFSGVLCASLLTITLSVAAHATELILDFNKVQMRSQQLAPGV 60
Pseudomonas sp. CTN-3------MPPGCSGLCSFVGLTMPLKFSGVLCASLLTITLSVAAHATELILDFNKVQMRSQQLAPGV 60
Rhodococcus sp. XF-8------MPPGCSGLCSFVGLTMPLKFSGVLCASLLTITLSVAAHATELILDFNKVQMRSQQLAPGV 60
Rhizobium sp. CTN-15-------MPLKFSGVLCASLLTITLSVAAHATELILDFNKVQMRSQQLAPGV 45
Ochrobactrum lupini------MPLKFSGVLCASLLTITLSVAAHATELILDFNKVQMRSQQLAPGV 45
Bordetella sp. CTN-10-------MPLKFSGVLCASLLTITLSVAAHATELILDFNKVOMRSOOLAPGV 45
Ochrobactrum sp. CTN-11--------MPLKFLGVLCASLLTITLSVAAHATELILDFNKVQMRSQQLAPGV 45
***********
Rhodococus sp. XF-6------YAHLPADSAELNAKGGVAGTSGGLIVGTRGAMLIETMLNRRLFDQVQALAKKEALGLPLL 120
Rhodococus sp. XF-3------YAHLPADSAELNAKGGVAGTSGGLIVGTRGAMLIETMLNRRLFDQVQALAKKEALGLPLL 120
Pseudomonas sp. CTN-3------YAHLPADSAELNAKGGVAGTSGGLIVGTRGAMLIETMLNRRLFDOVQALAKKEALGLPLL 120
Rhodococcus sp. XF-8------YAHLPADSAELNAKGGVAGTSGGLIVGTRGAMLIETMLNRRLFDQVQALAKKEALGLPLL 120
Rhizobium sp. CTN-15------YAHLPADSAELNAKGGVAGTSGGLIVGTRGAMLIETMLNRRLFDQVQALAKKEALGLPLL 105
Ochrobactrum lupini-------YAHLPADSAELNAKGGVAGTSGGLIVGTRGAMLIETMLNRRLFDQVQALAKKEALGLPLL 105
Bordetella sp. CTN-10------YAHLPADSAELNAKGGVAGTSGGLIVGTRGAMLIETMLNRRLFDQVQALTKKEALGLPLL 105
Ochrobactrum sp. CTN-11-------YAHLPADSAELNAKGGVAGTSGGLIVGTRGAMLIETMLNRRLFDQVQALAKKEALGLPLL 105
Caulobacter sp. CTN-14------YAHLPADSAELNAKGGVAGTSGGLIVGTRGAMLIETMLNRRLFDQVQALAKKEALGLPLL 105
Rhodococus sp. XF-6------YAVNT<mark>SYHGDH</mark>SYGNMYLKAPTRVIQSTKTRDYVDGHLADDKAFMVKNFGAGRGVEQITA 180
Rhodococus sp. XF-3-------YAVNT<mark>SYHGDH</mark>SYGNMYLKAPTRVIQSTKTRDYVDGHLADDKAFMVKNFGAGRGVEQITA 180
Pseudomonas sp. CTN-3------YAVNT<mark>SYHGDH</mark>SYGNMYLKAPTRVIOSTKTRDYVDGHLADDKAFMVKNFGAGRGVEOITA 180
Rhodococcus sp. XF-8-------YAVNT<mark>SYHGDH</mark>SYGNMYLKAPTRVIQSTKTRDYVDGHLADDKAFMMKNFGAGRGVEQITA 180
Rhizobium sp. CTN-15-------YAVNT<mark>SYHGDH</mark>SYGNMYLKAPTRVIQSTKTRDYVDGHLADDKAFMVKNFGAGRGVEQITA 165
Ochrobactrum lupini------YAVNT<mark>5YHGDH</mark>SYGNMYLKAPTRVIQSTKTRDYVDGHLADDKAFMVKNFGAGRGVEQITA 165
Bordetella sp. CTN-10-------YAVNT<mark>SYHGDH</mark>SYGNMYLKAPTRVIOSTKTRDYVDGHLADDKAFMVKNFGAGRGVEQITA 165
Ochrobactrum sp. CTN-11-------YAVNT<mark>SYHGDH</mark>SYGNMYLKAPTRVIQSTKTRDYVDGHLADDKAFMVKNFGAGRGVEQITA 165
Caulobacter sp. CTN-14------YAVNTSYHGDHSYGNMYLKAPTRVIQSTKTRDYVDGHLADDKAFMVKNFGAGRGVEQITA 165
                               Rhodococus sp. XF-6-------RTGDILVPPGGRVSVDLGGKTVEIIDFGFAQTGGDLFVWEPQSKVMWTGNAVVASKPALP 240
Rhodococus sp. XF-3------RTGDILVPPGGRVSVDLGGKTVEIIDFGFAQTGGDLFVWEPQSKVMWTGNAVVASKPALP 240
Pseudomonas sp. CTN-3------RTGDILVPPGGRVSVDLGGKTVEIIDFGFAQTGGDLFVWEPQSKVMWTGNAVVASKPALP 240
Rhodococcus sp. XF-8------RTGDILVPPGGRVSVDLGGKTVEIIDFGFAQTGGDLFVWEPQSKVMWTGNPVVASKPALP 240
Rhizobium sp. CTN-15------RTGDILVPPGGRVSVDLGGKTVEIIDFGFAQTGGDLFVWEPQSKVMWTGNAVVASKPALP 225
Ochrobactrum lupini------RTGDILVPPGGRVSVDLGGKTVEIIDFGFAQTGGDLFVWEPQSKVMWTGNSVVASKPALP 225
Bordetella sp. CTN-10------RTGDILVPPGGRVSVDLGGKTVEIIDFGFAQTGGDLFVWEPQSKVMWTGNAVVASKPALP 225
Ochrobactrum sp. CTN-11------RTGDILVPPGGRVSVDLGGKTVEIIDFGFAQTGGDLFVWEPQSKVMWTGNAVVASKPALP 225
Caulobacter sp. CTN-14------RTGDILVPPGGRVSVDLGGKTVEIIDFGFAQTGGDLFVWEPQSKVMWTGNSVVASKPALP 225
                               **************
Rhodococus sp. XF-6------WLLDGKLVETLATLQKVYDFLPPDATIVPGHGVPMAREGLRWHLDYLAAVQAGVKDALAR 300
Rhodococus sp. XF-3------WLLDGKLVETLATLQKVYDFLPPDATIVPGHGVPMAREGLRWHLDYLAAVQAGVKDALAR 300
Pseudomonas sp. CTN-3------WLLDGKLVETLATLQKVYDFLPPDATIVPGHGVPMAREGLRWHLDYLAAVQAGVKDALAR 300
Rhodococcus sp. XF-8------WLLDGKLVETLATLQKVYDFLPPDATIVPGHGVPMAREGLRWHLDYLAAVQAGVKDALAR 300
Rhizobium sp. CTN-15------WLLDGKLVETLATLQKVYDFLPPDATIVPGHGVPMAREGLRWHLDYLAAVQAGVKDALAR 285
Ochrobactrum lupini------WLLDGKLVETLATLQKVYDFLPPDATIVPGHGVPMAREGLRWHLDYLAAVQAGVKDALAR 285
Bordetella sp. CTN-10------WLLDGKLVETLATLQKVYDFLPPDATIVPGHGVPMAREGLRWHLDYLAAVQAGVKDALAR 285
Ochrobactrum sp. CTN-11-------WLLDGKLVETLATLQKVYDFLPPDATIVPGHGVPMAREGLRWHLDYLAAVQAGVKDALAR 285
Caulobacter sp. CTN-14------WLLDGKLVETLATLQKVYDFLPPDATIVPGHGVPMAREGLRWHLDYLAAVQAGVKDALAR 285
                               ** ****************
Rhodococus sp. XF-6------KLSLEQTVTELKMPEFRGYVLFDWVHPDLNVPAAYKDLAARP 342
Rhodococus sp. XF-3------KLSLEQTVTELKMPEFRGYVLFDWVHPDLNVPAAYKDLAARI 342
Pseudomonas sp. CTN-3------ 335
Rhodococcus sp. XF-8------KLSLEQTVTELKMPEFRGYVLFDWVHPDLNVPAAYKDLAARP 342
Rhizobium sp. CTN-15------KLSLEQTVTELKMPEFRGYVLFDWVHPDLNVPAAYKDLAARP 327
Ochrobactrum lupini------KLSLEQTVTELKMPEFRGYVLFDWVHPDLNVPAAYKDLAARP 327
Bordetella sp. CTN-10------KLSLEQTVTELKMPEFRGYVLFDWVHPDLNVPAAYKDLAARP 327
Ochrobactrum sp. CTN-11------KLSLEQTVTELKMPEFRGYVLFDWVHPDLNVPAAYKDLAARP 327
Caulobacter sp. CTN-14------KLSLEQTVTELKMPEFRGYVLFDWVHPDLNVPAAYKDLAARP 327
```

Figure 2

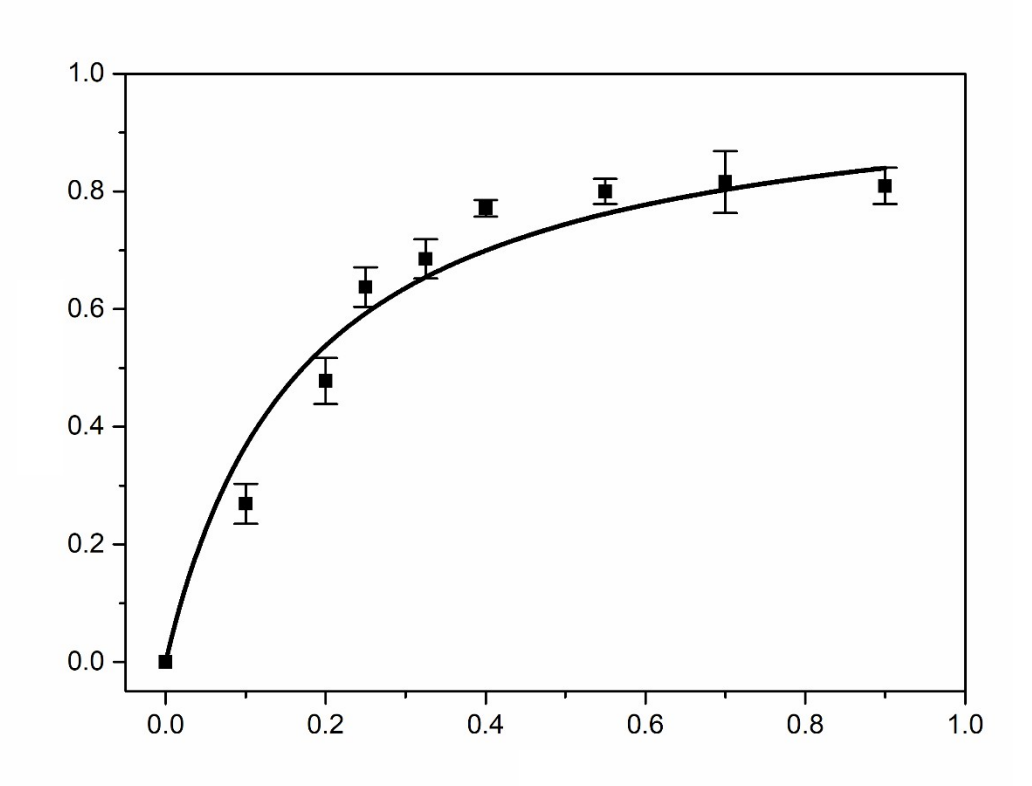
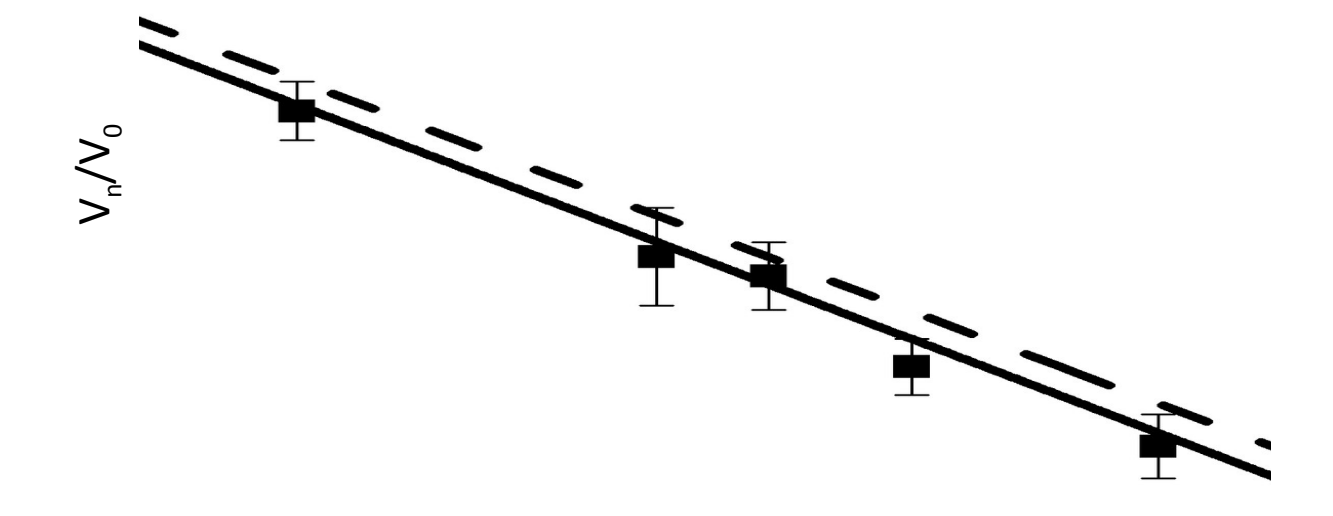


Figure 3

Figure 4



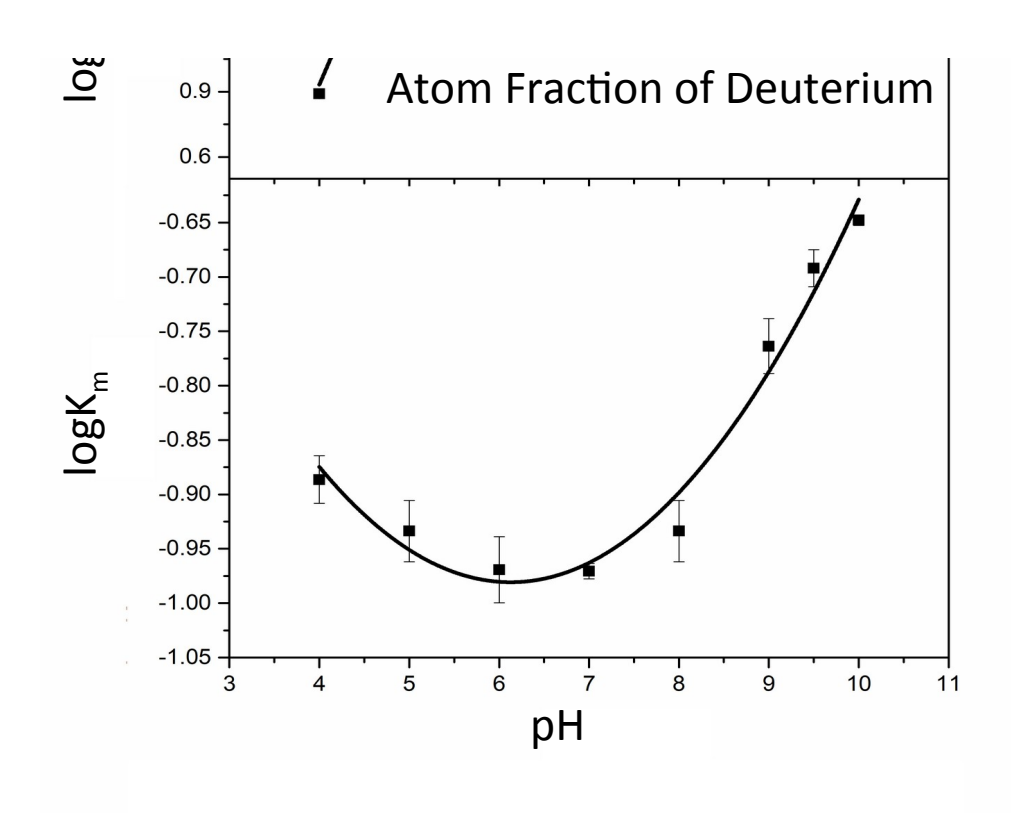


Figure 5

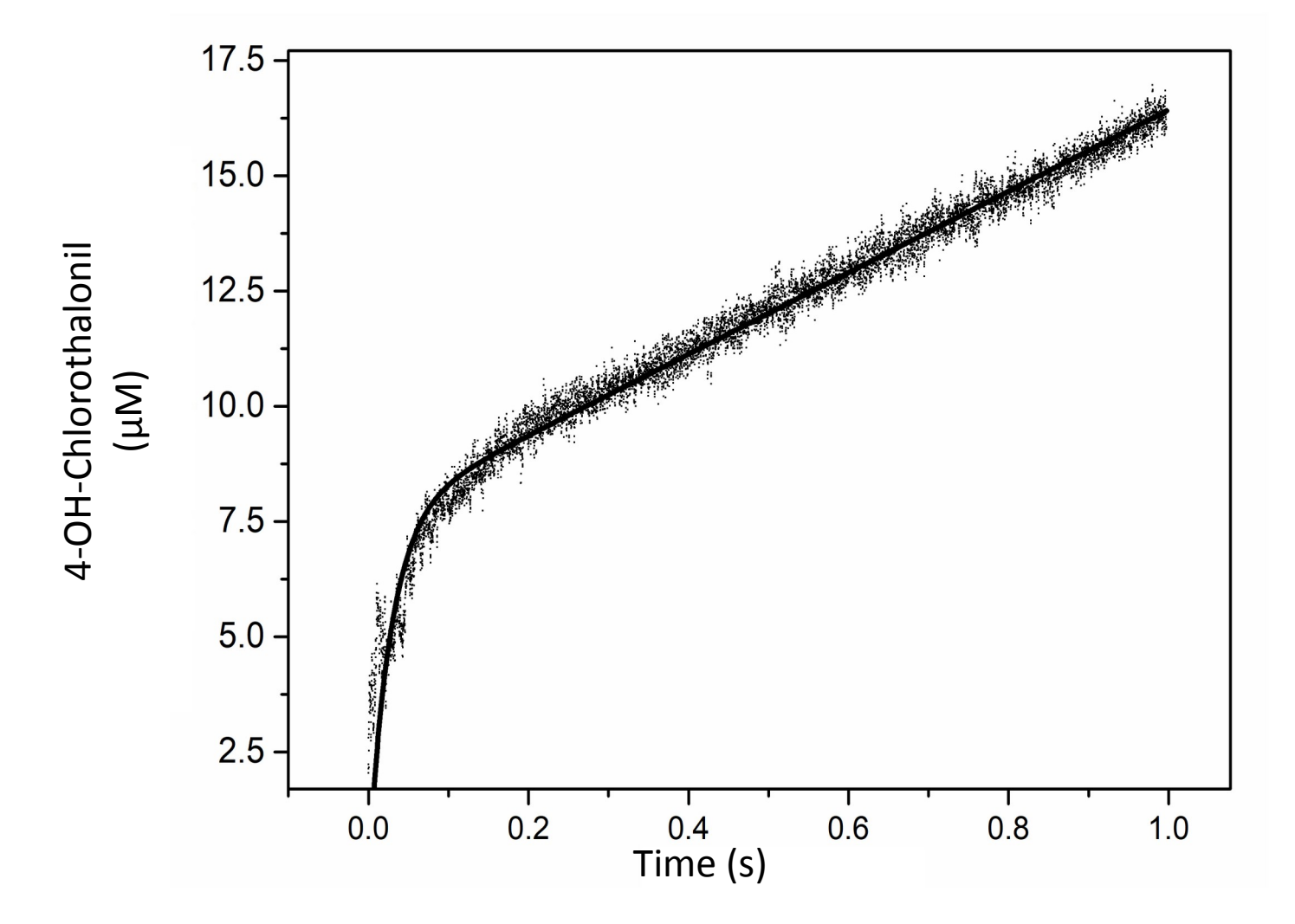


Figure 6

